Proceedings of the ASME 2009 International Design Engineering Technical Conferences & Computers and Information in Engineering Conference
IDETC/CIE 2009
August 30 - September 2, 2009, San Diego, California, USA

DETC2009-87808

A GENERALIZED CONSTRAINT MODEL FOR TWO-DIMENSIONAL BEAM FLEXURES

Shorya Awtar* and Shiladitya Sen
Precision Systems Design Laboratory
Mechanical Engineering, University of Michigan
Ann Arbor MI 48109

ABSTRACT

To utilize beam flexures in constraint-based flexure mechanism design, it is important to develop a qualitative and quantitative understanding of their constraint characteristics in terms of stiffness and error motions. This paper provides a highly generalized yet accurate closed-form load-displacement model for two-dimensional beam flexures, taking into account the nonlinearities arising from load equilibrium applied in the deformed configuration. In particular, stiffness and error motions are parametrically quantified in terms of elastic, load-stiffening, kinematic, and elastokinematic effects. The proposed beam constraint model incorporates any general loading conditions, boundary conditions, initial curvature, and beam shape. The accuracy and effectiveness of the proposed beam constraint model is verified extensively by non-linear Finite Elements Analysis.

1. INTRODUCTION AND BACKGROUND

Flexure mechanisms depend on elastic deformations to provide small but smooth and precise motions, and are essential elements of machine design [1-8]. Constraint-based design methods are commonly applied to flexure mechanisms because flexure elements behave like constraints [6-9]. A typical flexure element exhibits relatively small stiffness along certain directions, which may identified as its Degrees of Freedom (DoF), and relatively high stiffness along other directions, which act as its Degrees of Constraint (DoC). Fig.1 provides a comparison between representative traditional constraint elements and flexures that impose a single DoC between two rigid bodies, 1 and 2. The single DoC and associated two DoF, as indicated by the arrows, are realized by: the diameter of the rigid ball and two point contacts in case (A), the length of the rigid link and two traditional hinges in case (B), the length of the rigid link and two lumped compliance flexure hinges in case (C), and the length of the distributed compliance flexure beam in case (D).

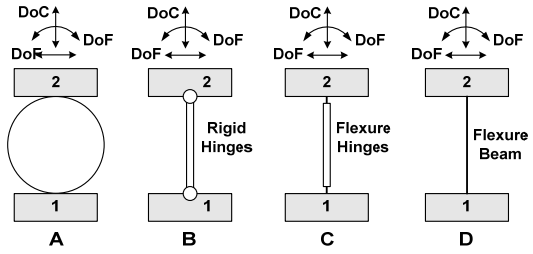

Fig. 1 Comparison of various Constraint Elements

An ideal constraint should provide zero error motion and infinite stiffness or load-bearing capacity along its DoC directions, and infinite motion range and zero stiffness along its DoF directions. While the traditional elements (A) and (B) come close to this idealization, the flexure elements (C) and (D) clearly deviate from ideal constraint behavior. The lumped-compliance flexure element (C) provides a relatively large stiffness in the DoC direction, but also exhibits a finite stiffness in the two DoF directions, thus limiting the motion range. Distributed compliance flexure beam (D), on the other hand, offers a relatively lower stiffness in the DoF directions, and therefore a greater motion range, but at the expense of stiffness in the DoC direction. Moreover, both flexure elements (C) and (D) exhibit an undesired parasitic error motion along the DoC direction. These observations not only highlight the non-ideal constraint behavior of the individual flexure elements but also

* Corresponding author (awtar@umich.edu, 734-615-0285)

the differences between the lumped and distributed compliance geometries, even though both are treated as equivalent in the traditional constraint-based design approaches.

Thus, to enable the deterministic constraint-based design of high performance flexure mechanisms, including their analysis, synthesis, and optimization, it is important to thoroughly characterize the constraint behavior of flexure elements in terms of their error motions and stiffness. This objective has been accomplished for a simple beam via a non-linear Beam Constraint Model, as reported in the prior literature [7, 10-11]. It has been shown that the deviation from ideal constraint behavior and associated performance tradeoffs arise due to the non-linearity associated with applying force equilibrium relations in the deformed beam configuration, which can be dominant even for small displacements.

Moving on from a uniform-thickness initially-straight simple beam, this paper extends the Beam Constraint Model to a completely generalized two-dimensional beam, incorporating any arbitrary end-loading conditions, end- displacement and slope conditions, initial curvature, beam shape, and temperature gradient along the beam length . Section 2 primes the reader by providing an overview of the previously derived constraint model for a simple beam. Additionally, new FEA verification and comparison with other modeling methods are presented. Section 3 covers the formulation and presents the non-linear load-displacement results for a uniform thickness beam with an initial slope and curvature. Section 4 does the same for an initially straight beam with a randomly varying cross-section along its length. Section 5 adds the contribution of a temperature distribution along the beam length to the Beam Constraint Model. This paper concludes in Section 6 with a summary of results and plans for future work.

2. BEAM CONSTRAINT MODEL (BCM)

The final results of the BCM for a simple beam are summarized below. For a detailed mathematical derivation and a discussion of the underlying assumptions, the reader is referred to the prior literature [7, 10-11].

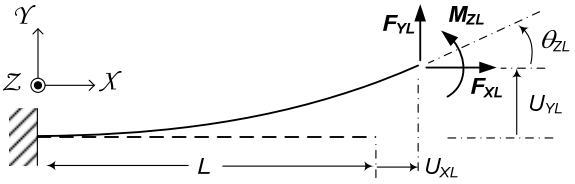

Fig. 2 Simple Beam Flexure

Fig.2 illustrates a simple beam (length: L, thickness: T, depth: H) subject to generalized end-loads $\boldsymbol{F_{XL}}$, $\boldsymbol{F_{YL}}$, and $\boldsymbol{M_{ZL}}$, resulting in end-displacements U_{XL} (DoC), U_{YL} (DoF), and θ_{ZL} (DoF), with respect to the coordinate frame XYZ. I_{ZZ} denotes the second moment of area about the bending axis Y; E denotes the Young's modulus for a state of plane-stress in XY, and plate modulus for a state of plane-strain in XY. Employing the Euler-Bernoulli and curvature linearization assumptions, applying load equilibrium in the beam's deformed condition, and truncating the resulting transcendental expressions to the first order in $\boldsymbol{F_{xL}}$, yields the following load-displacement relations:

$$\begin{bmatrix} \boldsymbol{F_{YL}} L^2/EI_{ZZ} \\ \boldsymbol{M_{ZL}} L/EI_{ZZ} \end{bmatrix} = \begin{bmatrix} k_{11}^{(0)} & k_{12}^{(0)} \\ k_{12}^{(0)} & k_{22}^{(0)} \end{bmatrix} \begin{bmatrix} \frac{U_{YL}}{L} \\ \theta_{ZL} \end{bmatrix} + \frac{\boldsymbol{F_{XL}} L^2}{EI_{ZZ}} \begin{bmatrix} k_{11}^{(1)} & k_{12}^{(1)} \\ k_{12}^{(1)} & k_{22}^{(1)} \end{bmatrix} \begin{bmatrix} \frac{U_{YL}}{L} \\ \theta_{ZL} \end{bmatrix} \quad (1)$$

$$\frac{U_{XL}}{L} = \frac{U_{XL}^{(e)}}{L} + \frac{U_{XL}^{(k)}}{L} + \frac{U_{XL}^{(e-k)}}{L} \quad (2)$$

$$\frac{U_{XL}^{(e)}}{L} = \frac{(T/L)^2}{12} \frac{\boldsymbol{F_{XL}} L^2}{EI_{ZZ}} \quad (3)$$

$$\frac{U_{XL}^{(k)}}{L} = \begin{bmatrix} \frac{U_{YL}}{L} & \theta_{ZL} \end{bmatrix} \begin{bmatrix} g_{11}^{(0)} & g_{12}^{(0)} \\ g_{12}^{(0)} & g_{22}^{(0)} \end{bmatrix} \begin{bmatrix} \frac{U_{YL}}{L} \\ \theta_{ZL} \end{bmatrix} \quad (4)$$

$$\frac{U_{XL}^{(e-k)}}{L} = \frac{\boldsymbol{F_{XL}} L^2}{EI_{ZZ}} \begin{bmatrix} \frac{U_{YL}}{L} & \theta_{ZL} \end{bmatrix} \begin{bmatrix} g_{11}^{(1)} & g_{12}^{(1)} \\ g_{12}^{(1)} & g_{22}^{(1)} \end{bmatrix} \begin{bmatrix} \frac{U_{YL}}{L} \\ \theta_{ZL} \end{bmatrix} \quad (5)$$

In this format, all loads, displacements, and stiffness terms are naturally normalized with respect to the beam parameters: displacements and lengths are normalized by the beam length L, forces by EI_{ZZ}/L^2, and moments by EI_{ZZ}/L.

$$\boldsymbol{f}_{x1} \triangleq \frac{\boldsymbol{F_{XL}} L^2}{EI_{ZZ}} \;;\; \boldsymbol{f}_{y1} \triangleq \frac{\boldsymbol{F_{YL}} L^2}{EI_{ZZ}} \;;\; \boldsymbol{m}_{z1} \triangleq \frac{\boldsymbol{M_{ZL}} L}{EI_{ZZ}}$$

$$u_{x1} \triangleq \frac{U_{XL}}{L} \;;\; u_{y1} \triangleq \frac{U_{YL}}{L} \;;\; \theta_{z1} \triangleq \theta_{ZL} \;;\; t \triangleq \frac{T}{L} \;;\; x \triangleq \frac{X}{L}$$

In the rest of this paper, lower case symbols are used to represent normalized variables and parameters, as per the above convention. The coefficients k's and g's are non-dimensional beam characteristic coefficients that are solely dependent on the beam shape and not its actual size. These coefficients take the following numerical values for a simple beam.

$k_{11}^{(0)}$	12	$k_{11}^{(1)}$	6/5	$g_{11}^{(0)}$	–3/5	$g_{11}^{(1)}$	1/700
$k_{12}^{(0)}$	–6	$k_{12}^{(1)}$	–1/10	$g_{12}^{(0)}$	1/20	$g_{12}^{(1)}$	–1/1400
$k_{22}^{(0)}$	4	$k_{22}^{(1)}$	2/15	$g_{22}^{(0)}$	–1/15	$g_{22}^{(1)}$	11/6300

Table 1. Characteristic Coefficients for a Simple Beam

The BCM helps characterize the constraint behavior of a simple beam flexure in terms of its stiffness and error motions. Error motions are the undesired motions in a flexure element or mechanism: any motion in a DoF direction, other than the intended DoF, is referred to as cross-axis coupling, and any motion along a DoC direction is referred to as parasitic error [7]. The first matrix term on the RHS of Eq.(1) provides the linear elastic stiffness in the DoF directions, while the second matrix captures load-stiffening, which results in a change in the effective stiffness in the DoF directions due to a DoC load. Eq.(2) shows that the DoC direction displacement, which is a parasitic error motion, is comprised of three terms. $U_{XL}^{(e)}$, given by Eq.(3), is a purely elastic component resulting from the stretching of the beam in the X direction. $U_{XL}^{(k)}$, given by Eq.(4),

represents a purely kinematic component dependent on the two DoF displacements, and arises from the constant beam arc-length constraint. $U_{XL}^{(e-k)}$, given by Eq.(5), represents an elastokinematic component, called so because of its elastic dependence on the DoC force $\boldsymbol{F_{XL}}$ and its kinematic dependence on the two DoF displacements. The elastokinematic component is also a consequence of the beam arc-length constraint, and arises due to a change in the beam deformation when $\boldsymbol{F_{xL}}$ is applied, even as U_{YL} and θ_{ZL} are held fixed. The kinematic component $U_{XL}^{(k)}$ dominates the DoC error motion and increases quadratically with increasing DoF displacements. The elastokinematic component of the DoC displacement, while small with respect to the purely kinematic component, is comparable to the purely elastic component and causes the DoC direction stiffness to drop quadratically from its nominal linear elastic value with increasing DoF displacements.

The BCM not only highlights the non-ideal constraint behavior of a beam flexure, it also reveals interdependence and fundamental tradeoffs between the DoF quality (large range, low stiffness) and DoC quality (high stiffness, low parasitic error). Moreover, unlike any other closed-form modeling approach, the BCM accommodates any generalized end-load and end-displacement conditions in a scale-independent, compact, and parametric format.

We next proceed to provide a comparison between the BCM for a simple beam and the corresponding non-linear FEA predications. An overview of the FEA procedure and settings used in this paper is provided in Appendix A. Fig.3 plots the elastic stiffness coefficients ($k_{11}^{(0)}, k_{12}^{(0)}$, and $k_{22}^{(0)}$) and load-stiffening coefficients ($k_{11}^{(1)}, k_{12}^{(1)}$, and $k_{22}^{(1)}$) versus the normalized DoF displacement u_{y1} or θ_{z1}. Similarly, Fig.4 plots the kinematic ($g_{11}^{(0)}, g_{12}^{(0)}$, and $g_{22}^{(0)}$) and elastokinematic ($g_{11}^{(1)}, g_{12}^{(1)}$, and $g_{22}^{(1)}$) coefficients. The BCM predictions are found to be within 6% of the FEA results for the DoF end-displacements (u_{y1} and θ_{z1}) in the range ±0.1 and the DoC end-load ($\boldsymbol{f_{x1}}$) in the range ±10. Any discrepancy can be entirely accounted for by: **A.** the non-linearity associated with the beam curvature [4], which is not incorporated in the BCM, and **B.** the truncation of higher order terms of $\boldsymbol{f_{x1}}$ in Eqs. (1) and (5). In general, this displacement and load range covers most practical flexure mechanism applications. The maximum error of 6% incurred over this range is a fair price for a greatly simplified and insightful closed-form parametric constraint model. An experimental validation of the BCM may be found in [12].

A quick comparison of the BCM with existing modeling techniques highlights its suitability for characterizing constraint behavior of flexures. A closed-form linear model, while simple and parametric, is obviously inadequate for constraint characterization because it fails to capture the load-stiffening, kinematic, or elastokinematic effects. Specific modeling exercises that do capture these pertinent nonlinearities are either mathematically too complex for flexure mechanism design [13], lack a broader generalization [14], or require numerical solution methods [15-16]. Elliptic integrals based solutions [17-19] do not provide closed-form results, are mathematically too complex for flexure mechanism design, and may be used only for uniform thickness beams.

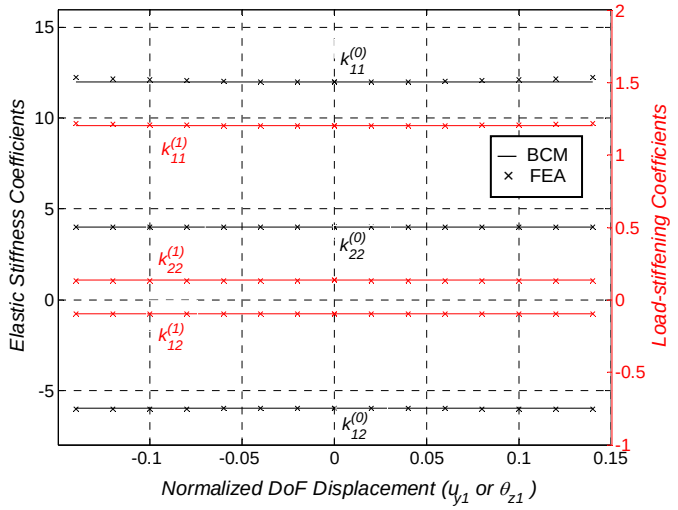

Fig. 3 Elastic Stiffness Coefficients and Load-Stiffening Coefficients for a Simple Beam: BCM vs. FEA

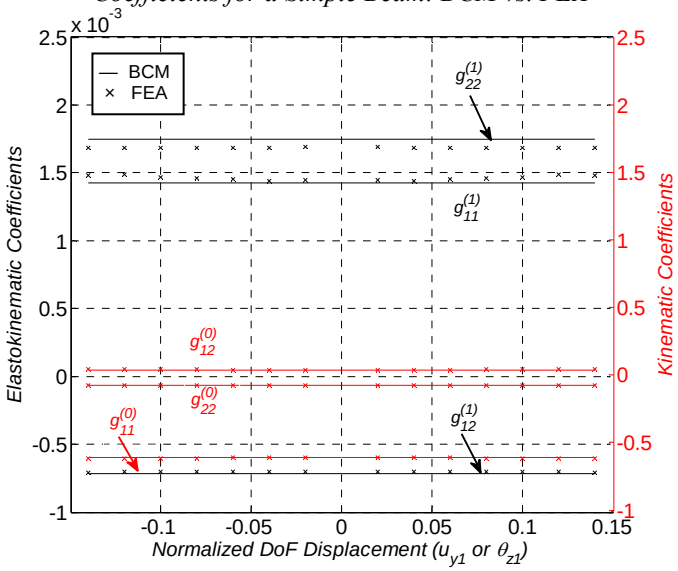

Fig. 4 Kinematic and Elastokinematic Coefficients for a Simple Beam: BCM vs. FEA

Pseudo Rigid Body Modeling (PRBM) offers a powerful parametric approach in capturing the large displacement behavior of beam flexures [20-22]. However, since the PRBM parameters are obtained via an optimization process that utilizes the exact elliptic integral based solution for a beam, these parameters have to be recomputed for every change in the loading conditions, boundary conditions, or initial beam curvature. Furthermore, for the optimal PRBM to be generated, an exact solution is needed *apriori*, which may not always be

possible for a variable cross-section beam. Also, while the PRBM captures load-stiffening and kinematic effects very accurately, its inherent lumped-compliance assumption precludes the elastokinematic effect. Since the elastokinematic effect plays a critical role in determining the DoC direction stiffness, error motions, and performance tradeoffs in flexures, the PRBM proves to be inadequate in characterizing their constraint behavior.

The attributes of these various modeling approaches are further highlighted and compared using the parallelogram flexure (Fig.5), comprised of two identical simple beams (L=250mm, T=5mm, H=50mm, W=75mm, E=210000Nmm^2)

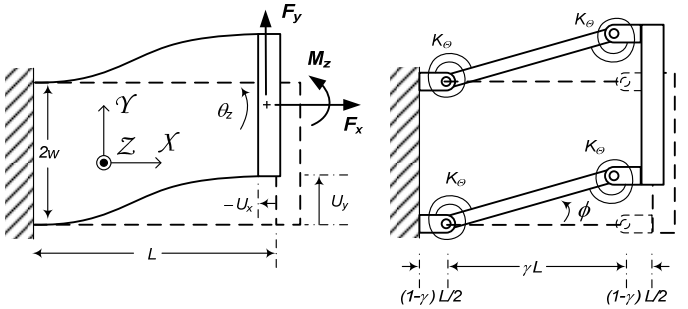

Fig. 5 Parallelogram Flexure and its Pseudo Rigid Body Model

Using the normalization convention introduced earlier, the linear model for this flexure module may be shown to be [2]:

$$\boldsymbol{f}_y = 24u_y \quad ; \quad u_x = 0 \quad ; \quad \theta_z = \frac{t^2}{24w^2}\left[\boldsymbol{m}_z + \frac{\boldsymbol{f}_y}{2}\right] \tag{6}$$

The non-linear load-displacement results for this flexure module have been derived using the BCM in the past [7,10]:

$$\boldsymbol{f}_y = \left(24 + 1.2\,\boldsymbol{f}_x\right)u_y \quad ; \quad u_x \approx \frac{t^2}{24}\boldsymbol{f}_x - \frac{3}{5}u_y^2 + \frac{1}{1400}u_y^2\boldsymbol{f}_x$$

$$\theta_z = \frac{1}{2w^2}\left(\frac{t^2}{12} + \frac{u_y^2}{700}\right)\left[\boldsymbol{m}_z + \boldsymbol{f}_y\frac{\left(12 + 0.1\,\boldsymbol{f}_x\right)}{\left(24 + 1.2\,\boldsymbol{f}_x\right)}\right] \tag{7}$$

A PRBM is also illustrated alongside the parallelogram flexure module in Fig.5. Assuming $\boldsymbol{m_z}$ and $\boldsymbol{f_x}$ to be zero, the model parameters are given by γ = 0.8517 and k_Θ = 2.65, and the load-displacement results are given by [4]:

$$\boldsymbol{f}_y\cos\phi - \boldsymbol{f}_x\sin\phi = 8k_\Theta\phi \quad ; \quad u_y = \gamma\sin\phi \quad ; \quad u_x = \gamma(\cos\phi - 1) \tag{8}$$

Clearly, the Y direction represents a DoF, while the X and Θ_Z directions represent DoC. Key constraint behavior predictions made by the above three models along with results from a non-linear FEA are plotted in Figs.6-8 over a u_y range of ± 0.15. Fig.6 plots the non-linear dependence of u_x (X DoC parasitic error motion) on u_y (Y DoF displacement) and illustrates that both the PRBM and BCM capture the kinematic effect in beams very accurately. Fig.7 plots the variation in the X direction (DoC) stiffness with u_y (Y DoF displacement). While the PRBM does not recognize any compliance in this DoC direction whatsoever, the linear model only captures the purely elastic stiffness component. The BCM is the only model that accurately predicts the elastokinematic effects, as verified by the FEA. Fig.8 plots θ_z (Θ_Z DoC parasitic error motion) with

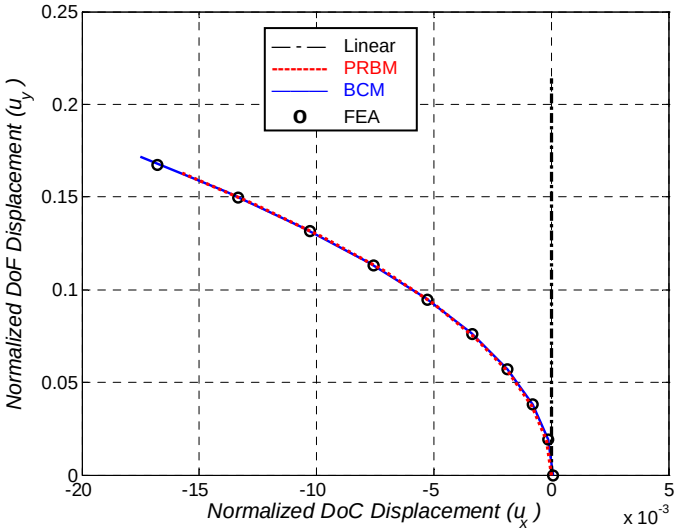

Fig. 6 Dependence of u_x (DoC) on u_y (DoF)

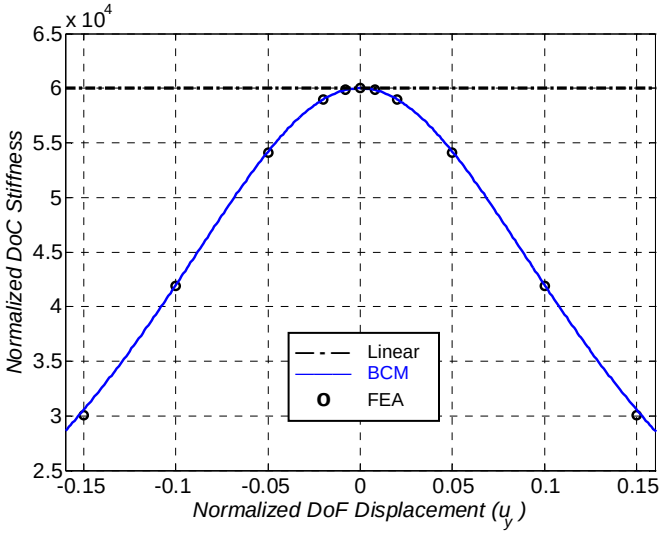

Fig. 7 Dependence of X direction (DoC) Stiffness on u_y (DoF)

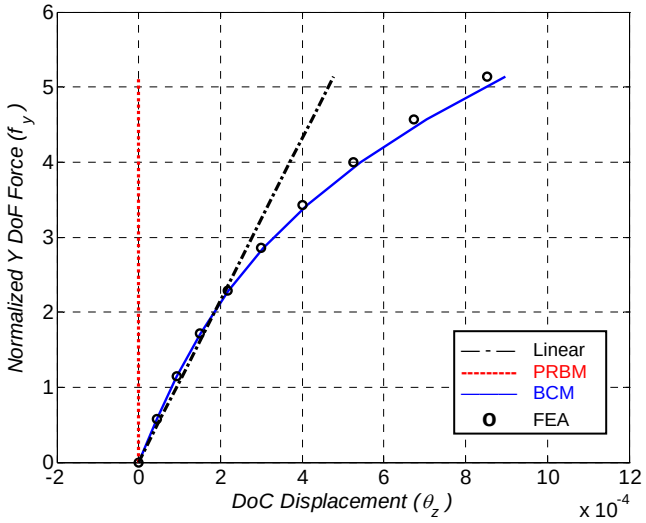

Fig. 8 Dependence of θ_z (Θ_Z DoC) on $\boldsymbol{f}_y$ (Y DoF)

increasing f_y (Y DoF force). The PRBM predicts zero yaw rotation of the rigid stage, while the linear model is valid only for small forces and displacements. However, the BCM accurately captures this parasitic error motion, also dominated by the elastokinematic effect, even for large values of the DoF force and displacement.

Thus, of the available options, the BCM is the only closed-form model that truly characterizes the constraint behavior of flexures in terms of stiffness variation and error motions, which demonstrates its importance in constraint-based flexure mechanism design.

3. UNIFORM-THICKNESS BEAM WITH GENERALIZED BOUNDARY CONDITIONS AND INITIAL CURVATURE

Next, we consider a uniform thickness beam with an arbitrary initial slope and an arbitrary but constant initial curvature. Note that choosing an arbitrary initial position simply shifts the coordinate frame of the beam by a constant value, and therefore is trivial. The objective is to capture these initial and boundary condition generalizations within the BCM, which so far has only dealt with a simple beam. The motivation for doing so is two-fold: 1. Analytically capture the consequence of manufacturing variations, e.g. in MEMS devices micro-fabricated beams can often assume an initially bent/curved to relieve material stresses, and 2. Use initial slope and curvature as additional design and optimization variables to achieve desired constraint characteristics.

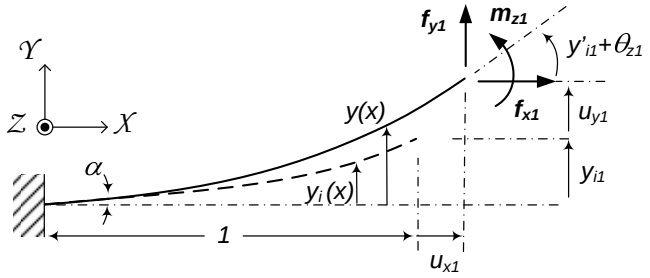

Fig. 9 Initially Slanted and Curved Beam

Fig.9 illustrates an initially slanted and curved beam with three generalized end-loads f_{x1}, f_{y1}, and m_{z1}, and three end-displacements u_{x1}, u_{y1}, and θ_{z1}, along the coordinate frame XYZ. All lower-case quantities are normalized with respect to beam parameters, as described earlier. The beam is assumed to have an initial slope α and an initial curvature of κ. For small initial slope and curvature (~ *0.1*), the Y and Θ_Z directions still serve as DoF, and the X direction is a DoC. The initial (unloaded and undeformed) beam configuration is denoted by $y_i(x)$, final (loaded and deformed) beam configuration is given by $y(x)$, and the beam deformation in the Y direction is given by $u_y(x)$, where

$$y_i(x) = \alpha x + \frac{\kappa}{2}x^2 \text{, and } y(x) = y_i(x) + u_y(x) \tag{9}$$

To derive the load-displacement relations for this beam flexure, Euler-Bernoulli and small curvature assumptions are made. The latter implies that the displacement, slope, and curvature of the beam in its deformed configuration remain of the order of *0.1*, so that the non-linearity associated with the beam curvature [x] may be dropped, as earlier. Thus, the normalized Euler's equation for this beam may be stated simply as $y''(x) = m_z(x)$, where the bending moment, $m_z(x)$, at a given cross section is computed by applying load equilibrium in the beam's deformed configuration:

$$m_z(x) = m_{z1} + f_{y1}\left(1 + u_{x1} - x\right) - f_{x1}\left(y_1 - y(x)\right) \tag{10}$$

Substituting this in the Euler's equation for the beam, and differentiating twice yields

$$\frac{d^4y(x)}{dx^4} = f_{x1}\frac{d^2y(x)}{dx^2} \tag{11}$$

For positive values of f_{x1}, the general solution for this fourth order linear differential equation may be stated as:

$$y(x) = c_1 + c_2x + c_3\sinh(rx) + c_4\cosh(rx), \text{ where } r^2 \triangleq f_{x1} \tag{12}$$

An analogous solution in trigonometric functions, instead of hyperbolic functions, exists for negative values of f_{x1}. The beam deflection, $u_y(x)$, therefore becomes:

$$\begin{aligned} u_y(x) &= y(x) - y_i(x) \\ &= c_1 + (c_2 - \alpha x) - \frac{\kappa}{2}x^2 + c_3\sinh(rx) + c_4\cosh(rx) \end{aligned} \tag{13}$$

Displacement boundary conditions at the two beam ends are given by:

$$u_y(0) = 0,\ u_y'(0) = 0,\ u_y(1) = u_{y1},\ u_y'(1) = \theta_{z1} \tag{14}$$

Using Euler's beam equation and Eqs.(9)-(10), the load boundary conditions at $x=1$ can be shown to be:

$$u_y'''(1) = -f_{y1} + f_{x1}\left(\theta_{z1} + \alpha + \kappa\right),\ u_y''(1) = m_{z1} \tag{15}$$

The above displacement and load boundary conditions may then be used to determine the coefficients c_1, c_2, c_3, and c_4, which ultimately lead to the following relations between the DoF direction end-loads and end-displacements.

$$\begin{bmatrix} f_{y1} \\ m_{z1} \end{bmatrix} = \begin{bmatrix} \dfrac{r^3\sinh(r)}{r\sinh(r) - 2\cosh(r) + 2} & \dfrac{r^2\{1 - \cosh(r)\}}{r\sinh(r) - 2\cosh(r) + 2} \\ \dfrac{r^2\{1 - \cosh(r)\}}{r\sinh(r) - 2\cosh(r) + 2} & \dfrac{r^2\cosh(r) - r\sinh(r)}{r\sinh(r) - 2\cosh(r) + 2} \end{bmatrix} \begin{bmatrix} u_{y1} \\ \theta_{z1} \end{bmatrix}$$
$$+ \begin{bmatrix} r^2 & -\dfrac{r^2}{2} \\ 0 & \dfrac{4\{\cosh(r) - r\sinh(r) - 1\} + r^2\{1 + \cosh(r)\}}{2\{r\sinh(r) - 2\cosh(r) + 2\}} \end{bmatrix} \begin{bmatrix} \alpha + \kappa \\ \kappa \end{bmatrix} \tag{16}$$

As is expected, setting $\alpha = \kappa = 0$, reduces the above expression to that for a simple beam [7, 10], prior to series expansion and truncation. As earlier, expanding the transcendental functions in the above matrices, and truncating 4th order or higher terms in r (or equivalently 2nd order or higher terms in f_{x1}), provides a great degree of simplification at less than 3% error over a comfortably large f_{x1} range (±5). The

simplified DoF direction force-displacement relations may thus be expressed as follows.

$$\begin{bmatrix} \boldsymbol{f}_{y1} \\ \boldsymbol{m}_{z1} \end{bmatrix} = \begin{bmatrix} 12 & -6 \\ -6 & 4 \end{bmatrix} \begin{bmatrix} u_{y1} \\ \theta_{z1} \end{bmatrix} + \boldsymbol{f}_{x1} \begin{bmatrix} 12 & -6 \\ -6 & 4 \end{bmatrix} \begin{bmatrix} u_{y1} \\ \theta_{z1} \end{bmatrix} + \boldsymbol{f}_{x1} \begin{bmatrix} 1 & -\frac{1}{2} \\ 0 & \frac{1}{12} \end{bmatrix} \begin{bmatrix} \alpha + \kappa \\ \kappa \end{bmatrix} \tag{17}$$

Clearly, the first two terms, in the above matrix equation, are identical to the elastic stiffness and load-stiffening terms in Eq.(1) for a simple beam. The last term is new and arises due to the initial slope and curvature. Even though this term might appear similar to the original load-stiffening term, it actually does not change the DoF stiffness values. The presence of α and κ simply shift the DoF load-displacement curves without affecting their slopes. This is corroborated to a high degree of accuracy by means of FEA for three different combinations of α and κ (Fig.10). The FEA is carried out over a relatively large u_{y1} range (± 0.1), with $\boldsymbol{f}_{x1}$ set to *5* and $\boldsymbol{m}_{z1}$ set to *0*. This constant shift for given beam geometry is a consequence of the fact that the DoC load $\boldsymbol{f}_{x1}$ produces additional bending moments along the beam length that are independent of the DoF displacements. The action of this load in the presence of DoF displacements indeed produces load-stiffing, but that is captured as usual by the second term in the above expression.

We next proceed to determine the DoC direction load-displacement expression for this flexure beam by imposing the following beam-arc length conservation relation.

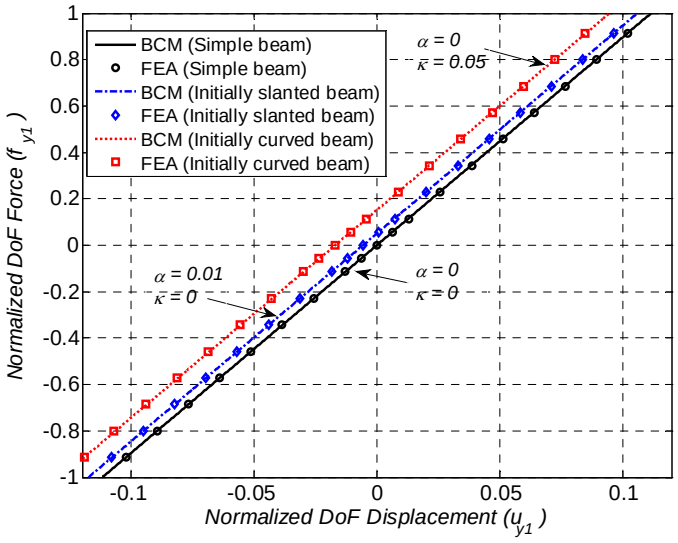

Fig. 10 DoF force ($\boldsymbol{f}_{y1}$) vs. DoF displacement (u_{y1}) for initially slanted or curved beams

$$\int_0^{1+u_{x1}^{(e)}} \left\{ 1 + \frac{1}{2} \left(y_i'(x) \right)^2 \right\} dx = \int_0^{1+u_{x1}} \left\{ 1 + \frac{1}{2} \left(u_y'(x) + y_i'(x) \right)^2 \right\} dx \tag{18}$$

The LHS is the total arc length, which is the sum of the initial length and the elastic elongation of the beam, $u_{x1}^{(e)}$. The RHS computes the total arc length after deformation, and hence the upper limit of integration changes to $(1+u_{x1})$. This DoC direction constraint equation may be solved using the solution for $u_y(x)$ derived earlier in Eq.(13), to yield the following relation between end-displacements and DoC end-load:

$$u_{x1} = \boldsymbol{f}_{x1} \frac{t^2}{12} - \begin{bmatrix} u_{y1} & \theta_{z1} \end{bmatrix} \begin{bmatrix} g_{11} & g_{12} \\ g_{21} & g_{22} \end{bmatrix} \begin{bmatrix} u_{y1} \\ \theta_{z1} \end{bmatrix} - \left(\alpha + \frac{\kappa}{2} \right) u_{y1} - g_{33} \left(\frac{\kappa}{2} \right) \theta_{z1} - g_{44} \left(\frac{\kappa}{2} \right)^2 \tag{19}$$

where,

$$g_{11} = -\frac{\boldsymbol{r}^2 \left\{ \cosh^2(\boldsymbol{r}) + \cosh(\boldsymbol{r}) - 2 \right\} - 3\boldsymbol{r} \sinh(\boldsymbol{r}) \left\{ \cosh(\boldsymbol{r}) - 1 \right\}}{2 \left\{ \boldsymbol{r} \sinh(\boldsymbol{r}) - 2\cosh(\boldsymbol{r}) + 2 \right\}^2} \quad , \text{where } \boldsymbol{r}^2 \triangleq \boldsymbol{f}_{x1}$$

$$g_{12} = g_{21} = \frac{\boldsymbol{r}^2 \left\{ \cosh(\boldsymbol{r}) - 1 \right\} + \boldsymbol{r} \sinh(\boldsymbol{r}) \left\{ \cosh(\boldsymbol{r}) - 1 \right\} - 4 \left\{ \cosh(\boldsymbol{r}) - 1 \right\}^2}{4 \left\{ \boldsymbol{r} \sinh(\boldsymbol{r}) - 2\cosh(\boldsymbol{r}) + 2 \right\}^2}$$

$$g_{22} = \frac{\boldsymbol{r}^3 - \boldsymbol{r}^2 \sinh(\boldsymbol{r}) \left\{ \cosh(\boldsymbol{r}) + 2 \right\} + 2\boldsymbol{r} \left\{ 2\cosh^2(\boldsymbol{r}) - \cosh(\boldsymbol{r}) - 1 \right\} - 2\sinh(\boldsymbol{r}) \left\{ \cosh(\boldsymbol{r}) - 1 \right\}}{4\boldsymbol{r} \left\{ \boldsymbol{r} \sinh(\boldsymbol{r}) - 2\cosh(\boldsymbol{r}) + 2 \right\}^2}$$

$$g_{33} = \frac{\boldsymbol{r}^3 \left\{ 1 + \cosh(\boldsymbol{r}) \right\} - \boldsymbol{r}^2 \sinh(\boldsymbol{r}) \left\{ 5 + \cosh(\boldsymbol{r}) \right\} + 4\boldsymbol{r} \left\{ \cosh^2(\boldsymbol{r}) + \cosh(\boldsymbol{r}) - 2 \right\} - 4\sinh(\boldsymbol{r}) \left\{ \cosh(\boldsymbol{r}) - 1 \right\}}{2\boldsymbol{r}_f \left\{ \boldsymbol{r} \sinh(\boldsymbol{r}) - 2\cosh(\boldsymbol{r}) + 2 \right\}^2}$$

$$g_{44} = \frac{\boldsymbol{r}^3 \left\{ \cosh^2(\boldsymbol{r}) + 3\cosh(\boldsymbol{r}) + 2 \right\} - \boldsymbol{r}^2 \sinh(\boldsymbol{r}) \left\{ 7\cosh(\boldsymbol{r}) + 11 \right\} + 4\boldsymbol{r} \left\{ 4\cosh^2(\boldsymbol{r}) + \cosh(\boldsymbol{r}) - 5 \right\} - 12\sinh(\boldsymbol{r}) \left\{ \cosh(\boldsymbol{r}) - 1 \right\}}{6\boldsymbol{r} \left\{ \boldsymbol{r} \sinh(\boldsymbol{r}) - 2\cosh(\boldsymbol{r}) + 2 \right\}^2}$$

Upon setting α and κ to zero, the above DoC direction relation reduces to the one obtained for a simple beam [7, 10], before series expansion and truncation. Next, as done for the DoF matrix equation, expanding the transcendental functions (*g*'s) and dropping higher order terms in $\boldsymbol{f_{x1}}$, provides a considerably more simple and insightful relation, at less than 3% error over $\boldsymbol{f_{x1}}$ in the range of ±5.

$$u_{x1} = \boldsymbol{f_{x1}}\frac{t^2}{12} + \begin{bmatrix} u_{y1} & \theta_{z1} \end{bmatrix} \begin{bmatrix} -\frac{3}{5} & \frac{1}{20} \\ \frac{1}{20} & -\frac{1}{15} \end{bmatrix} \begin{bmatrix} u_{y1} \\ \theta_{z1} \end{bmatrix}$$

$$+ \boldsymbol{f_{x1}} \begin{bmatrix} u_{y1} & \theta_{z1} \end{bmatrix} \begin{bmatrix} \frac{1}{700} & -\frac{1}{1400} \\ -\frac{1}{1400} & \frac{11}{6300} \end{bmatrix} \begin{bmatrix} u_{y1} \\ \theta_{z1} \end{bmatrix} \qquad (20)$$

$$-\left(\alpha + \frac{\kappa}{2}\right)u_{y1} - \frac{\kappa}{12}\theta_{z1} + \boldsymbol{f_{x1}}\frac{\kappa}{360}\theta_{z1} + \boldsymbol{f_{x1}}\frac{\kappa^2}{720}$$

The first (purely elastic), second (purely kinematic) and third (elastokinematic) terms in the above expression are identical to those obtained for the the simple beam (Eq.(2)). The effects of α and κ in the DoC direction are expressed via the last three terms. The fourth and fifth terms contribute to an extra purely kinematic component. Even though these terms do not exhibit a quadratic dependence on the DoF displacement like the previous kinematic terms, they are independent of the DoC load. The sixth term, which only depends on the initial curvature and not the slant, contributes to an extra elastokinematic effect, which again is not quadratic in the DoF displacement. However, this term produces a change in the DoC stiffness with increasing θ_{z1} displacement. The seventh and final term in the above expression is a new purely elastic term. Both the sixth and seventh terms arise due to the 'uncurling' of the beam deformation in the presence of a DoC load. In case of an initially slanted beam with no initial curvature ($\kappa = 0$), since this uncurling does not exist, there are no elastic or elastokinematic components when DoF displacements are zero.

These mathematical and physical observations are further verified via FEA for three different combinations of α and κ (Figs.11 and 12). Fig. 11 plots the parasitic error motion along the X DoC, u_{x1}, against the Y DoF displacement, u_{y1}. The corresponding FEA is carried out with $\boldsymbol{f_{x1}}$ set to *5* and $\boldsymbol{m_{z1}}$ set to *0*. Fig. 12 plots the X DoC stiffness against the Y DoF displacement, u_{y1}, and the FEA is carried out with $\boldsymbol{f_{x1}}$ set to *5* and θ_{z1} set to *0*. The FEA results are all found to be in good match with the generalized BCM developed in this section.

Thus, overall a uniform thickness beam flexure with initial slant and curvature continues to behave like a single DoC constraint element. The constraint characteristics along the DoF direction do not change considerably, but the DoC error motion as well stiffness is influence by the presence of additional linear, kinematic, and elastokinematic terms.

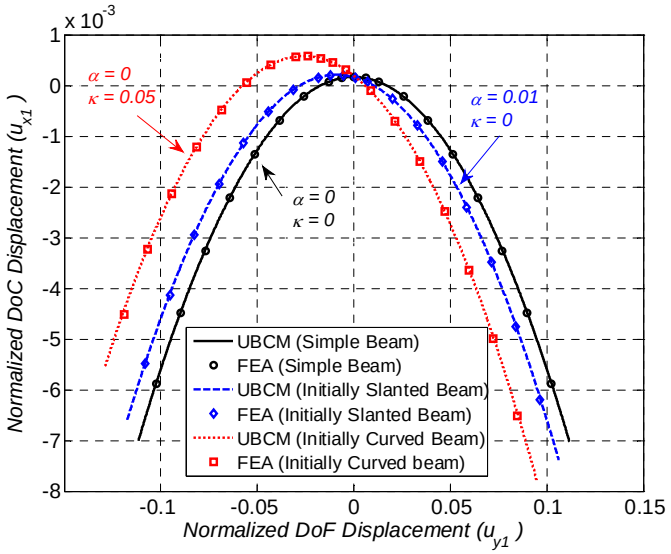

Fig. 11 DoC Displacement(u_{x1}) vs. DoF displacement (u_{y1}) for initially slanted or curved beams

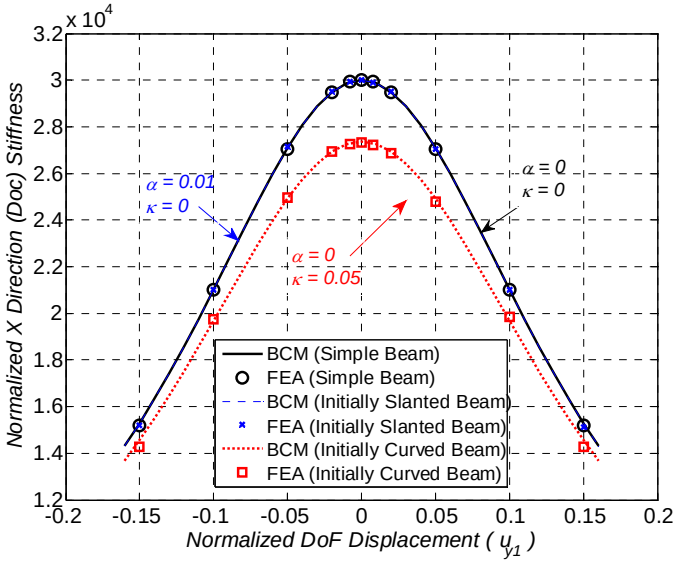

Fig. 12 DoC Stiffness vs. DoF displacement (u_{y1}) for initially slanted or curved beams

4. BEAM SHAPE GENERALIZATION

While in the previous two sections we have considered uniform thickness beams that may be initially straight, initially slanted, and/or initially curved, in this section we present a systematic process for developing the BCM for an initially straight beam with any generalized beam cross-section variation along its length. Such beam shape variation allows a non-uniform distribution of compliance along the beam length, and if the consequence of distributed compliance is analytically understood in terms of the beam constraint characteristics, one can carry out beam shape optimization.

Fig. 13 illustrates an initially straight beam with varying cross-section in its undeformed configuration subject to three generalized end-loads $\boldsymbol{f_{x1}}$, $\boldsymbol{f_{y1}}$, and $\boldsymbol{m_{z1}}$ along the coordinate

frame XYZ. The resulting three end-displacements u_{x1}, u_{y1}, and θ_{z1}, are not shown but are also along the same coordinate frame. As earlier, all lower-case quantities are normalized with respect to beam parameters. It is reasonable to assume that the undeformed neutral axis lies along the X axis. It is also obvious that the Y and Θ_z directions still serve as the Degrees of Freedom, while the X direction is a Degree of Constraint.

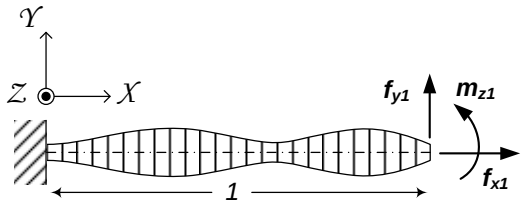

Fig.13 Straight Beam with Varying Cross-Section

Without any loss of generality, the second moment of area for the beam at given location x may be expressed as follows:

$$I(x) = I_{zz0}\left(1 + b_1 x + b_2 x^2 + \ldots + b_n x^n + \ldots\right) \tag{21}$$

The coefficients b's are called *beam shape parameters*, for obvious reasons. It is to be noted that the previously stated normalization is carried out using I_{zzo}, which is the second moment of area at $x=0$. Euler's equation for this beam may be determined by assuming small curvature and by applying load equilibrium in the deformed configuration

$$\left(1 + \sum_{i=1}^{\infty} b_i x^i\right)\frac{d^2 u_y(x)}{dx^2} = \boldsymbol{m}_{z1} + \boldsymbol{f}_{y1}(1-x) - \boldsymbol{f}_{x1}\left(u_{y1} - u_y(x)\right) \tag{22}$$

Upon choosing a new independent displacement variable given by $w(x) = \left\{\boldsymbol{m}_{z1} + \boldsymbol{f}_{y1}(1-x) - \boldsymbol{f}_{x1}\left(u_{y1} - u_y(x)\right)\right\}$, Eq. (22) reduces to the following homogenous form

$$\left(1 + \sum_{i=1}^{\infty} b_i x^i\right)\frac{d^2 w(x)}{dx^2} = \boldsymbol{f}_{x1} w(x) \tag{23}$$

This is a second order differential equation with variable coefficients that are analytic functions of x over the range [0 1], and therefore can be solved using the power series solution method [23]. It is noted here that the variable coefficient of $w(x)''$ is never zero because that would mean the second moment of area is zero. This means that the beam cross-section would vanish at that particular location, which is physically impractical. Since the coefficient of $w''(x)$ in Eq. (23) is a polynomial, its solution can be assumed to be an infinite polynomial series as follows.

$$w(x) = a_0 + a_1 x + a_2 x^2 + \ldots + a_n x^n + \ldots = \sum_{n=0}^{\infty} a_n x^n \tag{24}$$

The a's in the above expression are referred to as the *solution coefficients*. Substituting this assumed solution in the homogenized Euler beam equation (Eq.(23)) yields

$$\left(1 + \sum_{i=1}^{\infty} b_i x^i\right)\left(\sum_{n=0}^{\infty}\frac{(n+2)!}{n!}a_{n+2}x^n\right) = \sum_{m=0}^{\infty} a_m x^m \tag{25}$$

The above equation is true for all values of x and hence the coefficients of similar powers of x on the RHS and LHS can be equated. To equate the coefficients of the r^{th} power of x on both sides, Eq. (25) is differentiated r times and x is set to zero.

$$\left(\sum_{l=0}^{r}\left[{}^{r}c_l\left\{\frac{d^l}{dx^l}\left(\sum_{n=0}^{\infty} b_n x^n\right)\right\}\left\{\frac{d^{r-l}}{dx^{r-l}}\left(\sum_{m=0}^{\infty}\frac{(m+2)!}{m!}a_{m+2}x^m\right)\right\}\right]\right)_{x=0} = \left(\boldsymbol{f}_{x1}\frac{d^r}{dx^r}\left(\sum_{p=0}^{\infty} a_p x^p\right)\right)_{x=0}$$

$$\Rightarrow \sum_{l=0}^{r}\left[{}^{r}c_l\left\{l!(r-l+2)!\right\}b_l a_{r-l+2}\right] = \boldsymbol{f}_{x1} a_r r!$$

$$\Rightarrow a_{r+2} = \frac{\boldsymbol{f}_{x1} a_r}{(r+1)(r+2)} - \sum_{i=0}^{r-1}\left\{\frac{(r-i)(r-i+1)}{(r+1)(r+2)}a_{r-i+1}b_{i+1}\right\} \tag{26}$$

The previously undefined parameter b_0 is equal to *1* in the above equation. This equation relates the coefficient a_{r+2} with all its preceding coefficients, a_0 through a_{r+1}. The variables *l, m, p,* and *i* are dummy indices used for summation only. Using Eq.(26), the first four coefficients can be calculated as below.

$$a_0 = 1 \,.\, a_0 + 0 \,.\, a_1 \quad , \quad a_1 = 0 \,.\, a_0 + 1 \,.\, a_1$$
$$a_2 = \frac{1}{2!}\boldsymbol{f}_{x1} a_0 + 0 \,.\, a_1 \quad , \quad a_3 = -\frac{b_1}{3!}\boldsymbol{f}_{x1} a_0 + \frac{1!}{3!}\boldsymbol{f}_{x1} a_1 \tag{27}$$

From Eq.(27), it may be observed that the initial four coefficients can be all expressed in term of a_0 and a_1. By the method of induction, it is next shown that all a's can be similarly expressed as a linear combination of a_0 and a_1. Let us assume that for some j, each of the coefficients a_2 through a_j is represented in terms of a_0 and a_1:

$$a_n = h_{n,0} a_0 + h_{n,1} a_1 \qquad \forall\ 2 \le n \le j \tag{28}$$

Substituting Eq. (28) into Eq.(26), with $r+2 = j+1$, one may observe that a_{j+1} also turns out in terms of a_0 and a_1.

$$a_{j+1} = \frac{\boldsymbol{f}_{x1}\left(h_{j-1,0}a_0 + h_{j-1,1}a_1\right)}{(r+1)(r+2)} - \sum_{i=0}^{j-2}\left\{\frac{(j-i)(j-i-1)}{j(j+1)}h_{j-i,0}b_{i+1}\right\}a_0 - \sum_{i=0}^{j-2}\left\{\frac{(j-i)(j-i-1)}{j(j+1)}h_{j-i,1}b_{i+1}\right\}a_1 \tag{29}$$

.

Eq.(29) confirms that a_{j+1} can also be expressed in the form of Eq. (28). Thus, by the principle of induction, it is proven that all subsequent a's are of the form of Eq. (28). In this equation, $h_{n,0}$ represents the coefficient of a_0 in a_n, and similarly $h_{n,1}$ represents the coefficient of a_1 in a_n. Using Eq.(26), the following recursion formula for $h_{n,0}$ and $h_{n,1}$ may be obtained for $n>2$.

$$h_{n,0} = \frac{\boldsymbol{f}_{x1} h_{n-2,0}}{n(n-1)} - \sum_{i=0}^{n-3}\left\{\frac{(n-i-2)(n-i-1)}{n(n-1)}h_{n-i-1,0}b_{i+1}\right\}$$
$$h_{n,1} = \frac{\boldsymbol{f}_{x1} h_{n-2,1}}{n(n-1)} - \sum_{k=0}^{n-3}\left\{\frac{(n-k-2)(n-k-1)}{n(n-1)}h_{n-k-1,1}b_{k+1}\right\} \tag{30}$$

In the above formula, *i* and *k* are dummy variables used for summation. Also, it becomes evident that the coefficients $h_{n,0}$ and $h_{n,1}$ are functions of the beam shape parameters *b*'s and the DoC load $\boldsymbol{f}_{x1}$. Thus, using Eqs. (24), (28), and (30), the solution for *w(x)* and $u_y(x)$ may be stated as follows.

$$w(x) = a_0\left(1 + h_{2,0}x^2 + .. + h_{n,0}x^n + ..\right) + a_1\left(x + h_{2,1}x^2 + .. + h_{n,1}x^n + ..\right)$$

$$\Rightarrow u_y(x) = -\frac{1}{\boldsymbol{f}_{x1}}\left\{\boldsymbol{m}_{z1} + \boldsymbol{f}_{y1}(1-x)\right\} + u_{y1} + \frac{1}{\boldsymbol{f}_{x1}}\left\{a_0 s_0(x) + a_1 s_1(x)\right\}$$

$$\text{where, } s_0(x) \triangleq \left(1 + h_{2,0}x^2 + .. + h_{n,0}x^n + ..\right)$$
$$s_1(x) \triangleq \left(x + h_{2,1}x^2 + .. + h_{n,1}x^n + ..\right) \tag{31}$$

The series-solution, given by Eq.(31), is meaningful only when the series is convergent. If the second moment of inertia *I(x)*, in Eq.(21), is a q^{th} order polynomial, it can be shown that this series-solution is convergent at *x=1*, provided the convergence criteria, given in Eq.(32), is met. The reader is referred to Appendix B for the derivation of this condition.

$$\left\| roots\left(\rho^q + b_1\rho^{q-1} + ... + b_{q-1}\rho^1 + b_q = 0\right) \right\| < 1 \tag{32}$$

The displacement solution given in Eq.(31) has two arbitrary constants a_0 and a_1. This is expected since the Euler equation for the beam given by Eq. (23) is of second order. The two arbitrary constants are determined by applying the boundary conditions at the fixed end of the beam.

$$u_y(0) = 0,\ u_y'(0) = 0$$
$$\Rightarrow a_0 = \boldsymbol{m}_{z1} + \boldsymbol{f}_{y1} - \boldsymbol{f}_{x1}u_{y1},\ a_1 = -\boldsymbol{f}_{y1} \tag{33}$$

The DoF direction end-load end-displacement relations are obtained by setting *x=1* in the Eq.(31).

$$u_{y1} = u_y(1), \theta_{z1} = u_y'(1) \Rightarrow$$
$$u_{y1}\left\{\boldsymbol{f}_{x1}s_0(1)\right\} = \boldsymbol{f}_{y1}\left(s_0(1) - s_1(1)\right) + \boldsymbol{m}_{z1}\left(s_0(1) - 1\right) \text{ and} \tag{34}$$
$$\boldsymbol{f}_{x1}\theta_{z1} + \boldsymbol{f}_{x1}s_0'(1)u_{y1} = \boldsymbol{f}_{y1}\left(1 + s_0'(1) - s_1'(1)\right) + \boldsymbol{m}_{z1}s_0'(1)$$

This can be further converted to a matrix format as below.

$$\boldsymbol{f}_{x1}\begin{bmatrix} s_0(1) & 0 \\ s_0'(1) & 1 \end{bmatrix}\begin{Bmatrix} u_{y1} \\ \theta_{z1} \end{Bmatrix} = \begin{bmatrix} s_0(1) - s_1(1) & s_0(1) - 1 \\ 1 + s_0'(1) - s_1'(1) & s_0'(1) \end{bmatrix}\begin{Bmatrix} \boldsymbol{f}_{y1} \\ \boldsymbol{m}_{z1} \end{Bmatrix} \tag{35}$$

The above equation is solved to obtain the end loads in terms of end-displacements and the functions $s_0(x)$ and $s_1(x)$.

$$\begin{Bmatrix} \boldsymbol{f}_{y1} \\ \boldsymbol{m}_{z1} \end{Bmatrix} = \begin{bmatrix} k_{11} & k_{12} \\ k_{21} & k_{22} \end{bmatrix}\begin{Bmatrix} u_{y1} \\ \theta_{z1} \end{Bmatrix}$$

$$\text{where, } \quad k_{11} = \frac{\boldsymbol{f}_{x1}s_0'(1)}{\left\{s_0'(1) - s_1'(1) - s_0(1) + 2\right\}} \tag{36}$$

$$k_{12} = k_{21} = \frac{\boldsymbol{f}_{x1}\left\{1 - s_0(1)\right\}}{\left\{s_0'(1) - s_1'(1) - s_0(1) + 2\right\}}$$

$$k_{22} = \frac{\boldsymbol{f}_{x1}\left\{s_0(1) - s_1(1)\right\}}{\left\{s_0'(1) - s_1'(1) - s_0(1) + 2\right\}}$$

Maxwell's reciprocity principle, which requires the stiffness matrix to be symmetric, has been employed in going from Eq.(35) to Eq.(36). This principle requires the following to hold true at all times, which may be used to check the convergence and validity of the solution, as explained later.

$$s_1(1)s_0'(1) - s_0(1)s_1'(1) = -1 \tag{37}$$

The above relation can be easily verified to be true for the simple case in which the variation in cross-section is taken to be zero, i.e., $\forall$ *b*'s = 0. The expressions for $h_{n,0}$ and $h_{n,1}$, determined using Eq.(30), are given below.

$$h_{n,0} = \frac{\boldsymbol{f}_{x1}h_{n-2,0}}{n(n-1)}, \quad h_{j,1} = \frac{\boldsymbol{f}_{x1}h_{n-2,1}}{n(n-1)}$$
$$h_{0,0} = 1, \ h_{1,0} = 0, \quad h_{0,1} = 0, \quad h_{1,1} = 1$$
$$h_{2,0} = \frac{\boldsymbol{f}_{x1}}{2!}, \quad h_{2,1} = 0$$
$$h_{3,0} = 0, \quad h_{3,1} = \frac{\boldsymbol{f}_{x1}}{3!} \tag{38}$$
$$h_{4,0} = \frac{\boldsymbol{f}_{x1}^2}{4!}, \quad h_{4,1} = 0$$
$$h_{5,0} = 0, \quad h_{5,1} = \frac{\boldsymbol{f}_{x1}^2}{5!}$$

Substituting these values of $h_{n,0}$ and $h_{n,1}$ in Eq.(31), it is observed that the functions $s_0(x)$ and $s_1(x)$ are simply hyperbolic sine and cosine functions as given below.

$$s_0(x) = \left(1 + \frac{\boldsymbol{f}_{x1}}{2!}x^2 + \frac{\boldsymbol{f}_{x1}^2}{4!}x^4 ..\right) = \cosh\left(\sqrt{\boldsymbol{f}_{x1}}x\right)$$
$$s_1(x) = \left(x + \frac{\boldsymbol{f}_{x1}}{2!}x^3 + \frac{\boldsymbol{f}_{x1}^2}{2!}x^5 ..\right) = \frac{1}{\sqrt{\boldsymbol{f}_{x1}}}\sinh\left(\sqrt{\boldsymbol{f}_{x1}}x\right) \tag{39}$$

These values of $s_0(x)$ and $s_1(x)$ satisfy Eq.(37), thus verifying Maxwell's reciprocity principle. One may also check that substituting these hyperbolic functions into the load-displacement relations of Eq.(36) results in the exact transcendental relations for a simple beam [7, 10-11].

As mentioned earlier, the reciprocity principle may be used to determine the number of solution coefficients, *a*'s, to be used in Eq.(24). This is equivalent to choosing the highest power of *x* in $s_0(x)$ and $s_1(x)$ to be retained such that resulting $s_0(1)$ and $s_1(1)$ satisfy Eq.(37) within an acceptable margin of error.

Eq. (36) highlights the fact that even for a varying cross-section beam the DoF end-loads are related to the DoF end-displacements by a stiffness matrix that is a function of only the shape of the beam and the force in the DoC direction. This coupling of between the DoF direction stiffness matrix and the DoC direction force is similar to that seen in the simple beam (Eq.(1)). As is that case, the stiffness matrix may be expanded into an elastic stiffness matrix, a load-stiffening matrix, and higher order terms in the DoC force $\boldsymbol{f}_{x1}$.

Next, the DoC direction load-displacement relation may be formulated by applying the beam arc length constraint.

$$u_{x1} - u_{x1}^{(e)} = -\frac{1}{2}\int_0^1 \left\{u_y'(x)\right\}^2 dx \tag{40}$$

Differentiating the known $u_y(x)$ expression from Eq.(31), and rearranging it using Eq.(33), the following expression is obtained.

$$u_y'(x) = \frac{f_{y1}}{f_{x1}}\left\{1 + \frac{s_1(1)}{s_0(1)}s_0'(x) - s_1'(x)\right\} + \frac{m_{z1}}{f_{x1}}\frac{s_0'(x)}{s_0(1)} \tag{41}$$

This can be put into a matrix format and the resulting expression for $u_y'(x)^2$ is given below.

$$u_y'(x)^2 = \left\{\mathbf{f}_{y1} \quad \mathbf{m}_{z1}\right\}\begin{bmatrix} d_1 \\ d_2 \end{bmatrix}\begin{bmatrix} d_1 & d_2 \end{bmatrix}\begin{Bmatrix} \mathbf{f}_{y1} \\ \mathbf{m}_{z1} \end{Bmatrix}$$

$$\text{where,} \quad d_1 \triangleq \frac{1}{\mathbf{f}_{x1}}\left\{1 + \frac{s_1(1)}{s_0(1)}s_0'(x) - s_1'(x)\right\} \tag{42}$$

$$d_2 \triangleq \frac{1}{\mathbf{f}_{x1}}\frac{s_0'(x)}{s_0(1)}$$

Substituting Eq.(36) in the above expression, and substituting the resulting expression in Eq.(40), the constraint equation reduces to the following,

$$u_{x1} - u_{x1}^{(e)} = -\frac{1}{2}\left\{u_{y1} \quad \theta_{z1}\right\}\begin{bmatrix} k_{11} & k_{12} \\ k_{21} & k_{22} \end{bmatrix}\begin{bmatrix} d_{11} & d_{12} \\ d_{21} & d_{22} \end{bmatrix}\begin{bmatrix} k_{11} & k_{12} \\ k_{21} & k_{22} \end{bmatrix}\begin{Bmatrix} u_{y1} \\ \theta_{z1} \end{Bmatrix}$$

$$\Rightarrow u_{x1} = u_{x1}^{(e)} + \left\{u_{y1} \quad \theta_{z1}\right\}\begin{bmatrix} g_{11} & g_{12} \\ g_{21} & g_{22} \end{bmatrix}\begin{Bmatrix} u_{y1} \\ \theta_{z1} \end{Bmatrix} \tag{43}$$

$$\text{where,} \quad d_{11} \triangleq \int_0^1 \frac{1}{\mathbf{f}_{x1}^2}\left\{1 + \frac{s_1(1)}{s_0(1)}s_0'(x) - s_1'(x)\right\}^2 dx$$

$$d_{12} \triangleq d_{21} \triangleq \int_0^1 \frac{1}{\mathbf{f}_{x1}^2}\frac{s_0'(x)}{s_0(1)}\left\{1 + \frac{s_1(1)}{s_0(1)}s_0'(x) - s_1'(x)\right\}dx$$

$$d_{22} \triangleq \int_0^1 \left\{\frac{1}{\mathbf{f}_{x1}}\frac{s_0'(x)}{s_0(1)}\right\}^2 dx$$

Eq.(43) highlights the fact that even for a varying cross-section beam the DoC direction end-displacement is dependent on the DoF direction end-displacements and the DoC direction force $\mathbf{f}_{x1}$. This equation confirms that g_{11}, g_{12}, and g_{22} are functions of the beam shape and $\mathbf{f}_{x1}$ only. Setting the beam shape parameters b's to zero reduces this expression to the exact transcendental expression for a simple beam [7,10-11]. As is that case, the constraint matrix may be expanded into a kinematic terms matrix, and elastokinematic terms matrix, and higher order terms in $\mathbf{f}_{x1}$.

To recap the mathematical procedure presented above, the determination of the stiffness and constraint matrices is carried out as follows. The beam shape is quantified first by expressing the second moment of area of the beam as a function of x coordinate and beam shape parameters b's as in Eq.(21). The beam shape parameters are then used to check the convergence criteria (Eq.(32)). Once the convergence criteria is satisfied, the beam shape parameters may be used to calculate the solution coefficients a's in terms of the variables, $h_{n,0}$ and $h_{n,1}$, as per Eq. (30), and thus determine $s_0(x)$ and $s_1(x)$ as per Eq. (31). The functions $s_0(x)$ and $s_1(x)$ are then truncated in powers of x such that Maxwell's reciprocity criterion, given in Eq.(37), is satisfied within a certain acceptable error (e.g. 1%) for the given range of problem parameters: DoC force $\mathbf{f}_{x1}$ and the beam shape parameters. Finally these truncated functions $s_0(x)$ and $s_1(x)$ determine the load-displacement and constraint relations for the beam using Eq.(36) and (43), respectively.

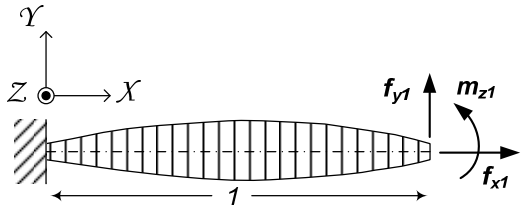

Fig.14 Straight Beam with a Sinusoidal Varying Area Moment of Inertia

The above proposed analysis procedure is illustrated by an example. A variable cross-section beam (Fig. 14) is described by Eq.(44). The resulting shape parameters b's are given in Table 2. Without any loss in generality, the area moment of inertia, as opposed to the beam thickness, is taken to a sinusoidal function.

$$I(x) = I_{zz0}\left\{1 + \frac{\eta}{100}\sin(\pi x)\right\} \tag{44}$$

b_1	$\eta\pi/100$	b_5	$\eta\pi^5/(5!100)$	b_9	$\eta\pi^9/(9!100)$
b_2	0	b_6	0	b_{10}	0
b_3	$-\eta\pi^3/3!$	b_7	$-\eta\pi^7/(7!100)$	b_{11}	$-\eta\pi^{11}/(11!100)$
b_4	0	b_8	0	b_{12}	0

Table 2. Shape parameters for a sinusoidally varying beam cross-section

The variable η is the highest percentage increase in the area moment of inertia which occurs at the middle of the beam. Using the twelve beam shape parameters given above the second moment of inertia function can be estimated with 0.01% accuracy for all 0<x<1. Hence, the higher order b's are neglected. It may be shown that the convergence criterion is satisfied by the shape parameters b's for $\eta < 10$. Next the h's and s's functions are calculated as previously described in Eq. (30) and Eq. (31) but are not presented here for brevity. The expressions for the functions $s_0(x)$ and $s_1(x)$ are truncated after the tenth power of x, satisfying Maxwell's reciprocity principle, Eq.(37), with less than 1% error for $\eta < 10$ and $\mathbf{f}_{x1}$ in the range ±5. The resulting stiffness matrix may be further expanded in terms of $\mathbf{f}_{x1}$, as follows:

$$\begin{Bmatrix} \boldsymbol{f}_{y1} \\ \boldsymbol{m}_{z1} \end{Bmatrix} = \begin{bmatrix} k_{11}^{(0)}(\eta) & k_{12}^{(0)}(\eta) \\ k_{21}^{(0)}(\eta) & k_{22}^{(0)}(\eta) \end{bmatrix} \begin{Bmatrix} u_{y1} \\ \theta_{z1} \end{Bmatrix} + \boldsymbol{f}_{x1} \begin{bmatrix} k_{11}^{(1)}(\eta) & k_{12}^{(1)}(\eta) \\ k_{21}^{(1)}(\eta) & k_{22}^{(1)}(\eta) \end{bmatrix} \begin{Bmatrix} u_{y1} \\ \theta_{z1} \end{Bmatrix} + \boldsymbol{f}_{x1}^{2} \begin{bmatrix} k_{11}^{(2)}(\eta) & k_{12}^{(2)}(\eta) \\ k_{21}^{(2)}(\eta) & k_{22}^{(2)}(\eta) \end{bmatrix} \begin{Bmatrix} u_{y1} \\ \theta_{z1} \end{Bmatrix} + \ldots \tag{45}$$

where, $\Phi(\eta) \triangleq (1 - 0.01\eta - 0.0002\eta^2)$

$$k_{11}^{(0)}(\eta) = \frac{12 - 0.304\eta + 0.0311\eta^2}{\Phi(\eta)^3}$$

$$k_{12}^{(0)}(\eta) = k_{21}^{(0)}(\eta) = \frac{-6 + 0.1676\eta - 0.01453\eta^2}{\Phi(\eta)^3}$$

$$k_{22}^{(0)}(\eta) = \frac{4 - 0.101\eta + 0.009\eta^2}{\Phi(\eta)^3}$$

$$k_{11}^{(1)}(\eta) = \frac{1.201 - 0.048\eta - 0.0103\eta^2}{\Phi(\eta)^3}$$

$$k_{12}^{(1)}(\eta) = k_{21}^{(1)}(\eta) = \frac{-0.1 + 0.009\eta + 0.0052\eta^2}{\Phi(\eta)^3}$$

$$k_{22}^{(1)}(\eta) = \frac{0.131 - 0.0082\eta + 0.0034\eta^2}{\Phi(\eta)^3}$$

$$k_{11}^{(2)}(\eta) = \frac{-0.00136 - 0.00094\eta + 0.0030\eta^2}{\Phi(\eta)^3}$$

$$k_{12}^{(2)}(\eta) = k_{21}^{(2)}(\eta) = \frac{0.00068 - 0.00098\eta - 0.00014\eta^2}{\Phi(\eta)^3}$$

$$k_{22}^{(2)}(\eta) = \frac{-0.00152 + 0.00072\eta + 0.00094\eta^2}{\Phi(\eta)^3}$$

Eq. (45) shows that the stiffness coefficients are function of the beam shape and DoC force $\boldsymbol{f}_{x1}$ only. The relation can be verified to match exactly with that of a simple beam if η is set to zero. The first matrix in Eq.(45) is the elastic stiffness matrix while the second matrix represents the load-stiffening matrix. The stiffness matrix associated with $\boldsymbol{f}_{x1}^2$ and higher order terms may be neglected with respect to the load-stiffening matrix, at the expense of 1-2% error over an $\boldsymbol{f}_{x1}$ range of ±5.

The constraint relation obtained for this particular case after similarly truncating matrices with second order and higher powers of $\boldsymbol{f}_{x1}$ is given below. It is interesting to note that the constraint relation has the same form as that for a simple beam, i.e., a summation of purely elastic term, a purely kinematic term, and an elastokinematic term.

$$u_{x1} = u_{x1}^{(e)} + \begin{Bmatrix} u_{y1} & \theta_{z1} \end{Bmatrix} \begin{bmatrix} g_{11}^{(0)}(\eta) & g_{12}^{(0)}(\eta) \\ g_{21}^{(0)}(\eta) & g_{22}^{(0)}(\eta) \end{bmatrix} \begin{Bmatrix} u_{y1} \\ \theta_{z1} \end{Bmatrix} + \boldsymbol{f}_{x1} \begin{Bmatrix} u_{y1} & \theta_{z1} \end{Bmatrix} \begin{bmatrix} g_{11}^{(1)}(\eta) & g_{12}^{(1)}(\eta) \\ g_{21}^{(1)}(\eta) & g_{22}^{(1)}(\eta) \end{bmatrix} \begin{Bmatrix} u_{y1} \\ \theta_{z1} \end{Bmatrix} \tag{46}$$

where, $g_{11}^{(0)}(\eta) = -\frac{1.201 - 0.048\eta - 0.0103\eta^2}{2\Phi(\eta)^3}$

$$g_{12}^{(0)}(\eta) = g_{21}^{(0)}(\eta) = -\frac{-0.1 + 0.009\eta + 0.0052\eta^2}{2\Phi(\eta)^3}$$

$$g_{22}^{(0)}(\eta) = -\frac{0.131 - 0.0082\eta + 0.0034\eta^2}{2\Phi(\eta)^3}$$

$$g_{11}^{(1)}(\eta) = -\frac{-0.00136 - 0.00094\eta + 0.0030\eta^2}{\Phi(\eta)^3}$$

$$g_{12}^{(1)}(\eta) = g_{21}^{(1)}(\eta) = -\frac{0.00068 - 0.00098\eta - 0.00014\eta^2}{\Phi(\eta)^3}$$

$$g_{22}^{(1)}(\eta) = -\frac{-0.00152 + 0.00072\eta + 0.00094\eta^2}{\Phi(\eta)^3}$$

The above example shows that the form of the load-displacement and constraint relations remains invariant in the BCM even for varying beam cross-sections. Thus, it may be concluded that BCM is valid for any generalized beam whose shape parameters are known. The beam characteristic coefficients in the BCM may be determined from the beam shape parameters using the above-described procedure. This generalization of the BCM also provides a useful tool for beam shape optimization. Furthermore, the solution obtained for the specific family of variable cross-section beam is closed-form in nature. Any change of parameters such end-loads, end-displacement, or beam shape (η) does not require a reformulation of the entire model.

5. BEAM SUBJECT TO THERMAL LOADING

Certain applications of flexure mechanisms may experience a considerable temperature range in their operating environment, e.g. compliant seals used in turbo-machinery (~ temperature range: 50-1200 °C). Other applications that require very high accuracy, such as high precision metrology instruments, are also very sensitive to temperature fluctuations in the ambient environment, which can cause undesired motion behavior. Flexure elements, generally comprising of thin section beams, have a lower thermal mass and therefore respond to temperature fluctuations faster than their surrounding rigid elements, for example. Therefore, it is of interest to incorporate the effect of a general temperature distribution along the beam length on the load-displacement relations, or equivalently the BCM, for any generalized beam. Considering the simple beam of Fig.2, the generalized temperature variation along its length may be given by $\Gamma(X)$.

The extension of any element dX will therefore be

$$\frac{dU_X}{dX} = \alpha_t \left(\Gamma(X) - \Gamma_a \right) \tag{47}$$

where, α_t is the coefficient of thermal expansion (CTE) for the material, and is generally of the order of 10^{-5} for metals [4]. Γ_a is the relevant ambient temperature. For most practical applications, $\Gamma(X) - \Gamma_a$ is of the order of *100* or less. Therefore,

the fractional change in beam length due to temperature fluctuations will be in the of the order of *0. 001* or less, which is very small compared to the normalized beam length *1*. Therefore, only the DoC displacement (u_{x1}), given by Eq.(2), is affected, while the DoF load-displacement relations given by Eq. (1) remain practically unchanged. The DoC direction displacement u_{x1}, is now given by:

$$\frac{U_{xL}}{L} = \frac{U_{xL}^{(e)}}{L} + \frac{U_{xL}^{(k)}}{L} + \frac{U_{xL}^{(e-k)}}{L} + \frac{U_{xL}^{(t)}}{L}$$

$$\text{where, } \frac{U_{xL}^{(t)}}{L} = \int_0^L \alpha_t \left(\Gamma(X) - \Gamma_a \right) \frac{dX}{L} \qquad (48)$$

Thus, in addition to the usual elastic, kinematic, and elastokinematic components in the parasitic error motion in the X DoC direction, there is a now a thermal component as well. While the above is shown for a simple beam, the same correction in beam length applies equally well to all other generalized beams considered here.

CONCLUSION

We have reviewed the Beam Constraint Model for a simple beam to highlight its advantages in capturing and accurately predicting the constraint characteristics of beam flexures. These advantages include a completely parametric, dimensionless, closed-form, and compact mathematical format that incorporates the load-stiffening, kinematic, and elastokinematic non-linearities. The accuracy of the BCM over fairly large DoC load and DoF displacement ranges is corroborated by non-linear FEA for a simple beam. A comparison with other modeling techniques is provided using the parallelogram flexure module as an example. Of the modeling techniques compared, the BCM is seen to be the only closed-from parametric model that captures all the pertinent stiffness variations and error motions, which ultimately characterize the constraint behavior of this module. Having shown these advantages, we then proceed to generalize the BCM to other beam geometries and shapes.

Generalization of the model to incorporate beams with initial slant and curvature is relatively straightforward. There are additional terms in the DoF and DoC direction load-displacement relations that show up. Effects of these generalizations are found to be more prominent for the DoC direction.

The generalization of BCM to incorporate any random beam shape is analytically more challenging. We employ a series based solution technique that involves considerable mathematical manipulation. However, once developed, this formulation is reduced to a set of systematic steps that may be carried out to obtain the beam characteristic coefficients in the BCM for any beam shape. It is shown that such a solution is possible as long as the beam shape parameters satisfy certain conditions, which physically correspond to keeping the beam shape variations small. While one convergence criteria to check for the validity of the series solution has been suggested, considerable further investigation is planned in this aspect of the solution methodology. Ultimately, we would like to place explicit bounds on individual beam shape parameters, as opposed to the presently proposed implicit criterion.

Finally, even though trivial, the effect of temperature variations along the beam length is also captured in the BCM.

The research presented in this provides a powerful means for capturing all possible beam shapes and geometries under one formulation – the Beam Constraint Model (BCM). We intend to use this formulation as the basis for constraint-based design that recognizes and leverages the deviations of flexure elements from ideal constraint behavior. The ability to vary the beam initial slant, initially curvature, or beam shape to achieve desired constraint characteristics by means of geometric optimization is an important first step in this direction. It is important to point out that, in addition to the constraint characteristics (stiffness and error motions) described here, maximum stress in a geometry also has to be taken into account in the design and optimization process for a given application. Stresses are not explicitly captured as part of the BCM, and are only indirectly reflected in the stiffness predictions.

Finally, while the formulation presented here is explicit, we are currently developing an energy-based formulation of the BCM so as to employ it in the modeling, analysis, and optimization of flexure mechanisms that may comprise complex arrangements of flexure beams.

REFERENCES

1. Jones, R.V., 1988, *Instruments and Experiences: Papers on Measurement and Instrument Design*, John Wiley & Sons, New York, NY
2. Smith S.T., 2000, *Flexures: Elements of Elastic Mechanisms*, Gordon and Breach Science Publishers
3. Slocum, A.H., 1992, *Precision Machine Design*, Society of Manufacturing Engineers, Dearborn, MI.
4. Howell L.L, 2001, *Compliant Mechanisms*, John Wiley & Sons
5. Lobontiu N., 2003, *Compliant Mechanisms: Design of Flexure Hinges*, CRC Press
6. Hale L.C., 1999, *Principles and Techniques for Designing Precision Machines*, Ph.D. Thesis, Massachusetts Institute of Technology, Cambridge MA
7. Awtar, S., 2004, *Analysis and Synthesis of Planer Kinematic XY Mechanisms*, Sc.D. thesis, Massachusetts Institute of Technology, Cambridge, MA
8. Blanding, D.K., 1999, *Exact Constraint: Machine Design Using Kinematic Principles*, ASME Press, New York, NY
9. Hopkins, J.B., 2005, *Design of Parallel Systems via Freedom and Constraint Topologies (FACT)*, MS Thesis, Massachusetts Institute of Technology, Cambridge, MA
10. Awtar, S., Slocum, A.H., and Sevincer, E., 2006, "Characteristics of Beam-based Flexure Modules", ASME Journal of Mechanical Design, 129 (6), pp 625-639
11. Awtar, S., and Sevincer, E, 2006, "Elastic Averaging in Flexure Mechanisms: A Multi-Parallelogram Flexure Case-

study", *Proc. ASME IDETC/CIE 2006*, Philadelphia, PA, Paper No. 99752
12. Awtar, S. and Slocum, A.H.,2007, "Constraint-based Design of Parallel Kinematic XY Flexure Mechanisms", *ASME Journal of Mechanical Design*, 129 (8)
13. Plainevaux, J.E., 1956, "Etude des deformations d'une lame de suspension elastique", Nuovo Cimento, 4, pp. 922-928.
14. Legtenberg, R., Groeneveld, A.W. and Elwenspoek, M., 1996, "Comb-drive Actuators for Large Displacements", Journal of Micromechanics and Microengineering, 6, pp. 320-329.
15. Haringx, J.A., "The Cross-Spring Pivot as a Constructional Element", Applied Science Research, A1(4), pp. 313-332.
16. Zelenika, S., and DeBona, F., 2002, "Analytical and Experimental Characterization of High Precision Flexural Pivots subjected to Lateral Loads", Precision Engineering, 26, pp. 381-388.
17. Bisshopp, K.E., and Drucker, D.C., 1945, "Large Deflection of Cantilever Beams", Quarterly of Applied Mathematics, 3(3), pp. 272-275.
18. Frisch-Fay, R., 1963, Flexible Bars, Butterworth, Washington DC.
19. Mattiasson, K., 1981, "Numerical Results from Large Deflection Beam and Frame Problems Analyzed by Means of Elliptic Integrals", International Journal for Numerical Methods in Engineering, 17, pp. 145-153.
20. Howell, L.L., and Midha, A., 1995, "Parametric Deflection Approximations for End-loaded, Large-deflection Beams in Compliant Mechanisms", ASME Journal of Mechanical Design, 117(1), pp. 156-165
21. Howell, L.L, and Midha, A., 1996, "Parametric Deflection Approximations for a Initially-curved, Large-deflection Beams in Compliant Mechanisms", Proc. ASME DETC 1996, MECH-1215
22. Howell, L.L., and Midha, A., and Norton, T.W., 1996, "Evaluation of Equivalent Spring Stiffness for use in a Pseudo-Rigid Body Model of Large-deflection Compliant Mechanisms", ASME Journal of Mechanical Design, 118(1), pp. 126-131
23. Simmons, G. F., and Robertson, J.S., 1991, *Differential Equations with Applications and Historical Notes*, 2nd Ed., McGraw Hill, pp.176-181

APPENDIX A: FEA PROCEDURE

The closed-form analytical expressions for the simple beam, slanted beam and the curved beam are validated by means of Finite Element Analysis performed in ANSYS. BEAM4 elements are used with consistent matrix and large displacement options turned on and shear coefficients set to zero. The material assumed is Stainless Steel, and typical values for Young's Modulus (*210,000* N.mm^{-2}) and Poisson's Ratio (*0.3*) are used. Beam length (L) = *250*mm, thickness (T) = *5*mm, and height (W) = *50*mm, are chosen for one of the FEA models. The undeformed neutral axis from the simple beam is taken along the x-axis. For all the beams meshing is done at 300 elements per 250mm. The convergence criteria for all FEA experiments is set to tolerance limits = 0.001 on the L2 norm. The values of DoF force typically used for Fig. 6-12 are 0-5kN. Normalized beam characteristic coefficients $k_{11}^{(0)}$ and $k_{22}^{(0)}$ in Fig.3 and 4 are measured one at time by setting u_{y1} and θ_{z1} alternately to 0 at zero DoC force. The corresponding load stiffness coefficients are measure by applying a DoC force but keeping the DoF displacements constants. By subtracting the two readings, $k_{11}^{(1)}$ and $k_{22}^{(1)}$ is determined. The coupling coefficient $k_{12}^{(0)}$ of u_{y1} and θ_{z1} are determined but proper algebraic sum of the displacement measurements from three cases, 1) $uy1=0$, θ_{z1}=known value 1, 2) $uy1$=known value 2, $\theta_{z1}=0$ and 3) $uy1$=known value 2, θ_{z1}=known value 1. The load stiffening coupling coefficients is similarly calculated by comparing the three sets of displacement at zero and nonzero DoC force values. The geometric constraint coefficients are calculated using a similar approach. The elastic stiffness is captured by setting u_{y1} and θ_{z1} to zero and applying a known DoC force. The kinematic geometric constraints coefficients are captured by the setting DoC force to zero. Finally the elastokinematic geometric constraint coefficients are calculated by setting DoF end displacements set to the same values as the case when purely kinematic displacement is measured. Using proper algebraic summation with purely kinematic and purely elastic case, the elastokinematic effect is isolated.

For the initially slanted beam in Fig. 10, 11 and 12 the base inclination angle is taken as 0.01 rad from the X-axis in the YZ plane. For the initial curved beam in Fig. 10, 11 and 12, the base angle is 0, while the radius of curvature is in 5mm. The center of curvature is located vertically 5mm from the base of the beam at co-ordinates (0,5). For measuring DoC stiffness for Fig. 7 and 12, the DoC force is varied between 1.5kN to 2kN keeping DoF end displacements u_{y1} and θ_{z1} fixed and measuring the DoC displacement u_{x1}.

APPENDIX B: CONVERGENCE CRITERION

For the power solution series given below to be a valid series, it has to be tested for convergence.

$$w(x) = a_0 + a_1 x + a_2 x^2 + \ldots + a_n x^n + \ldots \tag{49}$$

At $x=1$ the solution $w(1)$ in eq. (49) becomes a summation of all the coefficients. Thus for the solution to exist at $x=1$ the magnitude of the coefficients should be decreasing. Let us consider the recursion relation for the coefficients, restated here for the convenience of the reader.

$$\begin{aligned} a_{r+2} &= \frac{\boldsymbol{f}_{x1} a_r}{(r+1)(r+2)} - \sum_{i=0}^{r-1} \left\{ \frac{(r-i)(r-i+1)}{(r+1)(r+2)} a_{r-i+1} b_{i+1} \right\} \\ \Rightarrow \frac{a_{r+2}}{a_r} &= \frac{\boldsymbol{f}_{x1}}{(r+1)(r+2)} - \sum_{i=0}^{r-1} \left\{ \frac{(r-i)(r-i+1)}{(r+1)(r+2)} \frac{a_{r-i+1}}{a_r} b_{i+1} \right\} \end{aligned} \tag{50}$$

As r tends to infinity $1/r$ tends to zero. In this limiting situation one can derive Eq.(51). Also assuming that there are q shape

factors inputs, meaning $b_i = 0 \ \forall\, i > q$ the summation takes place from 0 to $q\text{-}1$ as given below.

$$\frac{a_{r+2}}{a_r} + \sum_{i=0}^{q-1}\left\{\frac{a_{r-i+1}}{a_r} b_{i+1}\right\} = 0 \tag{51}$$

Let the ratio between two consecutive coefficients be $\rho(r)$. The ratio should be less than 1 as r tends to infinity for the series to be convergent. Furthermore this ratio may either be decreasing or constant but less than 1 for the series to converge. If the ratio is less than 1 and decreasing then the series will converge fast. However, if the ratio is less than 1 but constant then the rate of convergence will be slower. Therefore if a series is proved to be convergent with a constant ratio assumption, it means that the series will only converge faster if the ratio was decreasing. Hence a constant ratio assumption solves for the worst case scenario and is adapted here.

$$\begin{aligned} &\frac{a_{r+2}}{a_{r+1}}\frac{a_{r+1}}{a_r} + \sum_{i=0}^{q-1}\left\{\frac{a_{r-i+1}}{a_{r-i+2}}\frac{a_{r-i+2}}{a_{r-i+3}}..\frac{a_{r-1}}{a_r} b_{i+1}\right\} = 0 \\ &\Rightarrow \rho^2 + \sum_{i=0}^{q-1}\left\{\frac{b_{i+1}}{\rho^{i-2}}\right\} = 0, \ where \ \rho \triangleq \frac{a_{r+2}}{a_{r+1}}, \forall\ r \ as \ r \to \infty \end{aligned} \tag{52}$$

The roots of equation are the possible ratios $\rho(r)$ as r tends to infinity. Only in the case when magnitudes of all the roots are less than one can the series be considered convergent at $x=1$. This criterion can be mathematically stated as below.

$$\left\| roots\left(\rho^q + b_1\rho^{q-1} + ... + b_{q-1}\rho^1 + b_q = 0\right) \right\| < 1 \tag{53}$$

However for practical purposes if the highest magnitude of the roots is less than 0.5, the series converges fast enough to truncate the series solution after 7-10 terms.